Publications

Observations and Modeling of Scintillation in the Vicinity of a Polar Cap Patch

Leslie J. Lamarche
SRI International

Kshitija B. Deshpande
Embry-Riddle Aeronautical University, deshpank@erau.edu

Matthew D. Zettergren
Embry-Riddle Aeronautical University, zettergm@erau.edu

Available online at:
www.swsc-journal.org

JSWSC

Topical Issue - Ionospheric plasma irregularities and their impact on radio systems

RESEARCH ARTICLE   **OPEN ACCESS**

Observations and modeling of scintillation in the vicinity of a polar cap patch

Leslie J. Lamarche[1,*] ⓘ, Kshitija B. Deshpande[2] ⓘ, and Matthew D. Zettergren[2] ⓘ

[1] Center for Geospace Studies, SRI International, Menlo Park, CA 94025, USA
[2] Department of Physical Sciences and Center for Space and Atmospheric Research (CSAR), Embry-Riddle Aeronautical University, Daytona Beach, FL 32114, USA

Abstract – Small-scale ionospheric plasma structures can cause scintillation in radio signals passing through the ionosphere. The relationship between the scintillated signal and how plasma structuring develops is complex. We model the development of small-scale plasma structuring in and around an idealized polar cap patch observed by the Resolute Bay Incoherent Scatter Radars (RISR) with the Geospace Environment Model for Ion-Neutral Interactions (GEMINI). Then, we simulate a signal passing through the resulting small-scale structuring with the Satellite-beacon Ionospheric-scintillation Global Model of the upper Atmosphere (SIGMA) to predict the scintillation characteristics that will be observed by a ground receiver at different stages of instability development. Finally, we compare the predicted signal characteristics with actual observations of scintillation from ground receivers in the vicinity of Resolute Bay. We interpret the results in terms of the nature of the small-scale plasma structuring in the ionosphere and how it impacts signals of different frequencies and attempt to infer information about the ionospheric plasma irregularity spectrum.

Keywords: scintillation / polar cap / ionosphere / gradient drift instability

1 Introduction

Radio signals passing through the ionosphere often experience ionospheric scintillation (rapid stochastic fluctuation of the amplitude and phase of the signal) due to non-uniform electron density in the ionosphere. Scintillation depends on the frequency of the signal and the scale of structuring, with GPS L-band frequencies being most sensitive to plasma irregularities in the 100 m – 10 km range (Kintner et al., 2007; Wang et al., 2016). Due to the societal importance of modern communication and navigation systems that depend on satellite-to-ground communication, it is critically important to understand what ionospheric conditions are responsible for potentially disruptive scintillation-scale plasma structures (Sojka, 2013).

The polar cap ionosphere, in general, is known to be dynamic and highly structured on a range of scales (Tsunoda, 1988), however, the exact relationship between different scales is still poorly understood. Large-scale structures such as polar cap patches and polar holes can be hundreds of kilometers across (Weber et al., 1984; Crowley et al., 1993; Crowley, 1996). These structures are thought to develop meso- and small-scale structures over time through various instability

mechanisms (Hosokawa et al., 2009). The gradient drift instability (GDI) is one of the primary drivers of structuring in the polar cap (Linson & Workman, 1970; Tsunoda, 1988; Burston et al., 2016). Linear theory suggests GDI is unstable on the trailing edge of polar cap patches and stable on the leading edge, leading to a greater degree of small-scale structuring on the trailing edge of patches (Keskinen & Ossakow, 1981; Makarevich, 2014). Some observations support this asymmetrical development of structuring in patches (Weber et al., 1984; Milan et al., 2002; Hosokawa et al., 2016), while others demonstrate a significant amount of leading-edge structuring (Kivanç & Heelis, 1997; Coley & Heelis, 1998; Thayyil et al., 2021). Specifically, GPS observations have shown scintillation in the vicinity of patches regardless of whether the ray path is passing through the leading or trailing edge, suggesting that other instability mechanisms may be important (Coker et al., 2004; Jin et al., 2014, 2017; Jayachandran et al., 2017). Other studies have also found that nonlinear instability development and turbulent wave interaction may be critical to how meso- and small-scale structures form in the polar cap (Gondarenko & Guzdar, 2006a; Spicher et al., 2015; Lamarche et al., 2020).

A number of modeling studies have examined the linear and nonlinear behavior of gradient-drift instability as related to polar cap patches. Guzdar et al. (1998) conducted 2D and

---

*Corresponding author: leslie.lamarche@sri.com

3D simulations and demonstrated that the evolution of patches is impacted by whether one model has local (i.e., confined F-region) versus nonlocal effects. The full ionospheric altitude distribution of fields and plasma needs to be considered in analyzing detailed patch dynamics. These studies were later extended by Gondarenko & Guzdar (1999), who added in the effects of ionospheric ion inertia, which plays the role of slowing patch growth, consistent with prior 2D studies (Mitchell Jr. et al., 1985; Huba et al., 1988), and found good correspondence between density fluctuations in the model and those observed by the DE 2 satellite (Gondarenko & Guzdar, 2004a, 2004b). The effects of shearing (Gondarenko & Guzdar, 2006a) and time-dependent forcing (Gondarenko & Guzdar, 2006b) have likewise been shown to impact density and electric field fluctuations arising from the ionosphere turbulence. Deshpande & Zettergren (2019) have coupled a physics-based model of GDI to a radio propagation model and shown that the instability can generate density irregularities that can explain some aspects of polar cap phase scintillation. Collectively these theoretical studies paint a complicated picture of patch evolution and its connection to irregularities and scintillation – patches are highly sensitive to the initial distribution of ionospheric plasma (including large-scale gradients, seeding structures, and altitude profiles), as well as the temporal effects like variable forcing and ion inertia (Deshpande et al., 2021). Very little has been done to explore the parameter spaces of how various patch features (gradients, absolute density, seeding, mesoscale propagation) impact scintillation; most modeling studies lack data constraints for these.

Scintillation on the ground is seen as fluctuations in a received radio signal and occurs due to the propagation of radio waves through irregular media. Both refractive and diffractive effects contribute to scintillation, and the Fresnel radius (r_F) is usually cited as the critical scale where signal diffraction becomes significant. This study uses equation (1) for the Fresnel radius rather than the far-field approximation presented in other GPS scintillation work (i.e., Yeh & Liu, 1982; Kintner et al., 2007) that assumes the transmitter is far from the scattering volume:

$$r_F = \sqrt{\frac{\lambda r_1 r_2}{r_1 + r_2}}. \tag{1}$$

Here, λ is the signal wavelength, and r_1 (r_2) is the distance from the transmitter (receiver) to the scattering volume.

The turbulent density in the ionosphere needs to be accurately presented to represent the underlying instability mechanism for a rigorous scintillation simulation of an ionospheric event. Historically, spectral models have been used to represent irregularities (Shkarofsky, 1968; Costa & Kelley, 1977); however, these models do not capture the plasma dynamics at different stages of an instability's development, viz., instabilities progress through various physical stages related to seeding, linear growth, nonlinear evolution, and saturation/turbulence. Physics-based models are a promising avenue to capture this temporal evolution and develop a better understanding of how scintillation is related to polar cap patches and their motion and evolution.

In this study, we aim to investigate how scintillation-scale structures develop nonlinearly under realistic polar cap conditions – to the extent that we can constrain these with our data – and examine how well current nonlinear first principle models can replicate spectral characteristics of observed scintillation signals. We will also compare scintillation at three frequencies and consider if differences between these signals allow us to infer characteristics of the intrinsic plasma structuring that causes scintillation.

2 Methodology

We examine a single case of a polar patch observed traveling through the polar cap and use state-of-the-art models guided by direct observations to predict the scintillation signatures in the local region. These expected scintillation signatures are then compared with high-rate scintillation data from co-located multi-frequency receivers in the polar region. This study uses a variety of instrumentation and numerical models discussed below. Due to observation and model constraints, the modeled patch is still idealized but characterized by direct measurements.

2.1 RISR

The Resolute Bay Observatory (RBO) is home to two Advanced Modular Incoherent Scatter Radars (AMISR) (Kelly & Heinselman, 2009): Resolute Bay Incoherent Scatter Radar North (RISR-N) (Bahcivan et al., 2010) and Resolute Bay Incoherent Scatter Radar Canada (RISR-C) (Gillies et al., 2016) bore-sighted approximately along magnetic north and magnetic south, respectively. Incoherent scatter radars are ground-based instruments that can measure the electron density, electron and ion temperature, and ion line-of-sight (LoS) velocity of plasma in the ionosphere. AMISR radars utilize electronic beam steering to rapidly scan through a relatively large number of pointing directions, allowing the radar to effectively measure plasma parameters in a local volume simultaneously. This capability allows us to image polar patches and other large-scale ionospheric structures in three dimensions (3D). The standard AMISR processing routine gates the lag product array into auto-correlation functions, and determines the plasma parameters within each range gate through the nonlinear least-squares fitting of the autocorrelation functions. This analysis assumes the fitted parameters are slowly vary in range over the pulse length and in time over the integration period. This study focuses on F-region dynamics, so only long pulse data are presented.

For the event considered here, both RISR-N and RISR-C were operating in the 51-beam "Imaginglp" mode. At 300 km height, the combined field-of-view (FoV) in this mode is approximately 1000 km long and 500 km wide, with an average beam separation of about 58 km. In addition to the general size, shape, and peak electron density (NmF2) and altitude (hmF2) of the patch from the volumetric density measurements, full plasma convection velocity vectors can be derived from the AMISR LoS velocity measurements by assuming relatively stable convection over the FoV (Heinselman & Nicolls, 2008).

2.2 GEMINI-SIGMA

The GEMINI (Geospace Environment Model of Ion-Neutral Interactions) is a three-dimensional (3D) multifluid-electrodynamic model of ionospheric plasma instabilities (Zettergren & Snively, 2015). GEMINI includes electrodynamic

processes and aeronomical transport that are required to model the generation of ionospheric fluid instabilities, such as GDI and KHI. It has been interfaced with a full three-dimensional (3D) electromagnetic wave forward propagation model (Deshpande et al., 2014), SIGMA (Satellite-beacon Ionospheric- scintillation Global Model of the upper Atmosphere) (Deshpande & Zettergren, 2019; Spicher et al., 2020). SIGMA can simulate the propagation of a radio signal through irregular media in the ionosphere, which comprises effects such as scattering, diffraction, wave refraction, and reflection through an arbitrary density field - including a turbulent plasma simulated by a physics-based model like GEMINI. SIGMA handles the propagation of a radio frequency signal from a moving satellite to the ground through the ionosphere anywhere on the globe (Deshpande et al., 2014). The multiple phase screens (MPS) approach is an established method of model effects of ionospheric irregularities on radio signals (Knepp, 1983). This method divides the ionosphere into phase screen(s), which only impart phase fluctuations on the incoming wave. The signal undergoes further phase and amplitude fluctuations both during the free space propagation between the screens and from the bottom of the irregularity to the ground.

The propagation in SIGMA works in a local geomagnetic continuously displaced coordinate system (CDCS) along the LoS vector, similar to that described by Rino (2010). GEMINI density cubes are spatially linearly interpolated at the desired sampling times and then fed into SIGMA with the side of the cube between 50 and 100 km. The GEMINI simulation in this paper uses a ~100 m grid, however due to numerical diffusion and limits of the modeled physical processes, the smallest realistically resolvable scale is ~200–250 m. Inside SIGMA, the density cubes are transformed into phase screens using a split-step method, and the forward propagation equation is solved for the incoming LoS signal (Rino, 2010). The signal undergoes scattering inside the density cube (or the ionospheric irregularity), and the complex signal received on the ground has a distorted phase and power. The signal phase and power at the receiver as a function of time are recorded as the high rate signal phase and power time series, which we filter with the same techniques as the observations.

2.3 Scintillation data

GPS scintillation data are obtained from the CHAIN (Canadian High Arctic Ionospheric Network) receiver at Resolute Bay (Jayachandran et al., 2009). For this study, we are using the high-rate (50 Hz) amplitude and phase data from the L1 (1575.420 MHz) signal. RBO also hosts a CERTO (Coherent Electromagnetic Radio Tomography) receiver (Bernhardt & Siefring, 2006; Siefring et al., 2015). This receiver can detect 50 Hz VHF (150.012 MHz) and UHF (400.032 MHz) signals transmitted from beacons on a variety of low-earth orbit satellites. For this study, the beacon was on CASSIOPE, with an orbiting altitude of ~650 km. Power is recorded from VHF and UHF, but the phase is only measured in VHF relative to the UHF channel. These time series are detrended by subtracting a cubic polynomial fit to the data, then applying a sixth-order high-pass Butterworth filter with a 0.1 Hz cut-off to remove any low-frequency components associated with either satellite motion or large-scale (not scintillation-causing) plasma structures. The Fresnel scale (Eq. (1)) for the L1 (1575.420 MHz), UHF
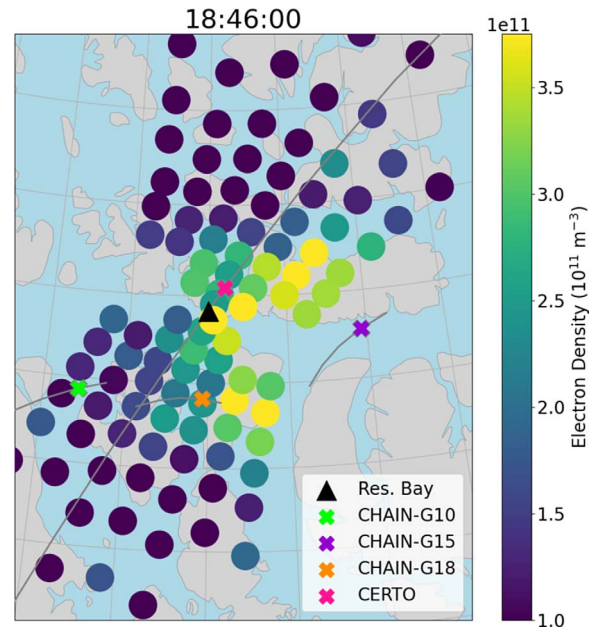

Fig. 1. Polar patch considered in this case study as seen in the RISR FoV. RISR beam positions and measured densities at 300 km are shown, as well as the tracks from 18:00 to 19:00 (grey line) and positions at 18:46 (thick "x") of the IPPs from the four conjunctions considered in this study. Both the CHAIN and CERTO receivers are located in Resolute Bay, but CHAIN detects signals transmitted by various GPS satellites while CERTO detects that from the CASSIOPE beacon. Included are CHAIN-GPS G10 (green), CHAIN-GPS G15 (purple), CHAIN-GPS G18 (orange), and CERTO-CASSIOPE (pink). An animation of the entire period the patch was observed is available in the Supplementary materials.

(400.032 MHz), and VHF (150.012 MHz) signals in the ionosphere at F-region height are approximately 237 m, 348 m, and 568 m, respectively.

3 Event overview

The polar cap patch considered in this study was observed with RISR on November 21, 2017, from 18:30 to 19:00 UT. The polar cap patch was moving roughly antisunwards across the polar cap, traversing first through RISR-C, then RISR-N in about 30 min. Figure 1 shows the electron density measured by RISR at the F-region peak at 18:46 UT, where the patch is clearly visible on the right side of both radar's FoV. Additionally, there were four scintillation observations with receivers in Resolute Bay in the vicinity of this patch. Three were from the CHAIN receiver and correspond to signals transmitted from three different GPS satellites (PRNs 10, 15, and 18) and one from the CERTO receiver (corresponding to the beacon transmitter on CASSIOPE). The Ionospheric Pierce Points (IPPs) of the satellite-receiver line from each of these events are also plotted in Figure 1 as "x"s. Passes are identified by the receiver network (CHAIN or CERTO) for consistency with the receiver data shown later in this article. An animation of the motion of the patch and the four IPPs is available in the
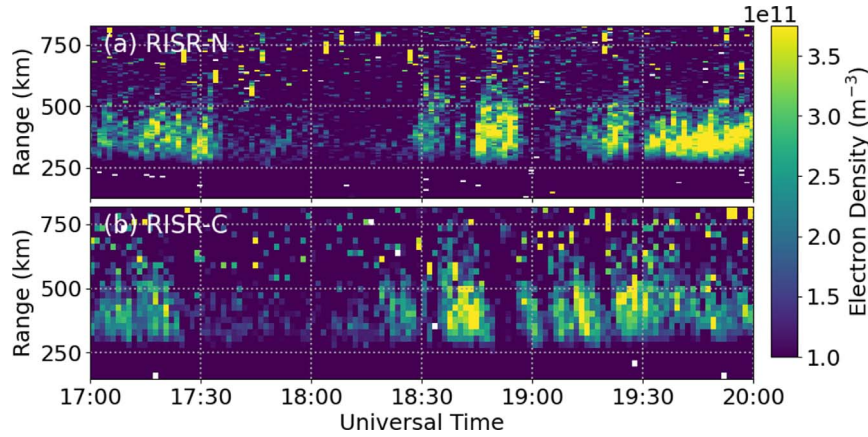
Fig. 2. Electron density measurements from beams in the center of the RISR-N (a) and RISR-C (b) FoVs for the period around the event considered in this paper. The patch considered in this study is the large density enhancement that appears between 18:30 and 19:00 in both radars.

Table 1. Basic characteristics of the polar cap patch considered in this study.

Characteristic	Value
Horizontal extent	415 km
Vertical extent	175 km
h_mF_2	335 km
N_mF_2	4.94×10^{11} m^{-3}
Interior Te	1250 K
Exterior Te	2000 K
Velocity	875 m/s

Supplemental Material (S1). The CERTO IPP quickly transverses the entire RISR FoV between 18:43 and 18:48 UT. The CHAIN IPPs are much slower, and the patch effectively moves over them as it convects across the polar cap. Figure 2 shows electron density from beams near the centers of the FoVs of both RISR-N (Fig. 2a) and RISR-C (Fig. 2b). Because the patch is moving north–east, it is visible in the RISR-C data first (at around 18:35 UT) before moving into the RISR-N FoV at around 18:45 UT. Note that this patch is one of a series of density enhancements passing through the polar cap. Table 1 describes the approximate size of the patch and the plasma parameters that characterize it and are used to initialize the GEMINI simulation. Technically, the initial patch parameters should be measured at the patch's conception in the cusp, but this is outside the combined RISR FoV. The patch edge gradient scale length is critical to the GDI growth rate, but it cannot be calculated reliably from RISR as the beam separation, even in imaging modes, is significantly greater than the gradient scale length expected to drive GDI (discussed in detail in Sect. 6). This event was chosen because it was a relatively clear and isolated density enhancement that abides by most traditional definitions of polar cap patches (a plasma density enhancement at least twice the background density) (Weber et al., 1984; Perry & St.-Maurice, 2018; Ren et al., 2018). Furthermore, it occurred when both RISR-N and RISR-C were operating in an imaging mode in conjunction with several independent scintillation observations. There are only a limited number of

close conjunctions of all systems, so we choose to focus on a single example with high-quality data for this study.

4 Simulating irregularity development and scintillation

In this work, we use the GEMINI ionospheric model (Zettergren & Snively, 2015; Zettergren et al., 2015; Deshpande & Zettergren, 2019) to simulate instability on an idealized patch with approximate characteristics derived from the RISR observations. A 3D Cartesian grid spanning $90 \leq z \leq 1000$, $-350 \leq x \leq 350$, $-25 \leq y \leq 25$ (km) is used for this simulation; the y-direction is assumed periodic, and the magnetic field is taken to be in the $-z$-direction (northern hemisphere). The initial plasma density patch in the model is given by:

$$n_e(x,y,z,t_0) = n_{e0}(z) + 4n_{e0}(z)\left[\frac{1}{2}\tanh\left(\frac{x-x_1}{\ell}\right) - \frac{1}{2}\tanh\left(\frac{x-x_2}{\ell}\right)\right]$$

$$(2)$$

$$v_x(x,y,z,t) = v_0. \qquad (3)$$

Here, $v_0 \approx 875$ m/s and $n_{e0} \approx 1.2 \times 10^{11}$ m^{-3} so that the patch velocity and peak density (4 times the background) are approximately equivalent to the observed values in Table 1. The gradient scale length for this simulation is $\ell = 10$ km and the patch horizontal extent is taken to be $x_1 = -220$ km; $x_2 = -140$ km. The gradient scale length was not calculated from RISR observations and instead intuited from the approximate time scale of the event and previous sounding rocket and modeling studies. This is discussed in detail in Section 6. Note that the patch extent is different from the data but does not affect the initiation and progression of the instability over time scales of interest to this work and greatly reduces the number of grid points required to simulate the irregularities – the patch is some 400 km across, yet we only attempt to simulate instability at the edges, viz. where it is initiated in this model. The model resolution, $\Delta x \times \Delta y$, for this simulation is ~125 × 100 m. This polar cap patch is seeded with additive white Gaussian noise
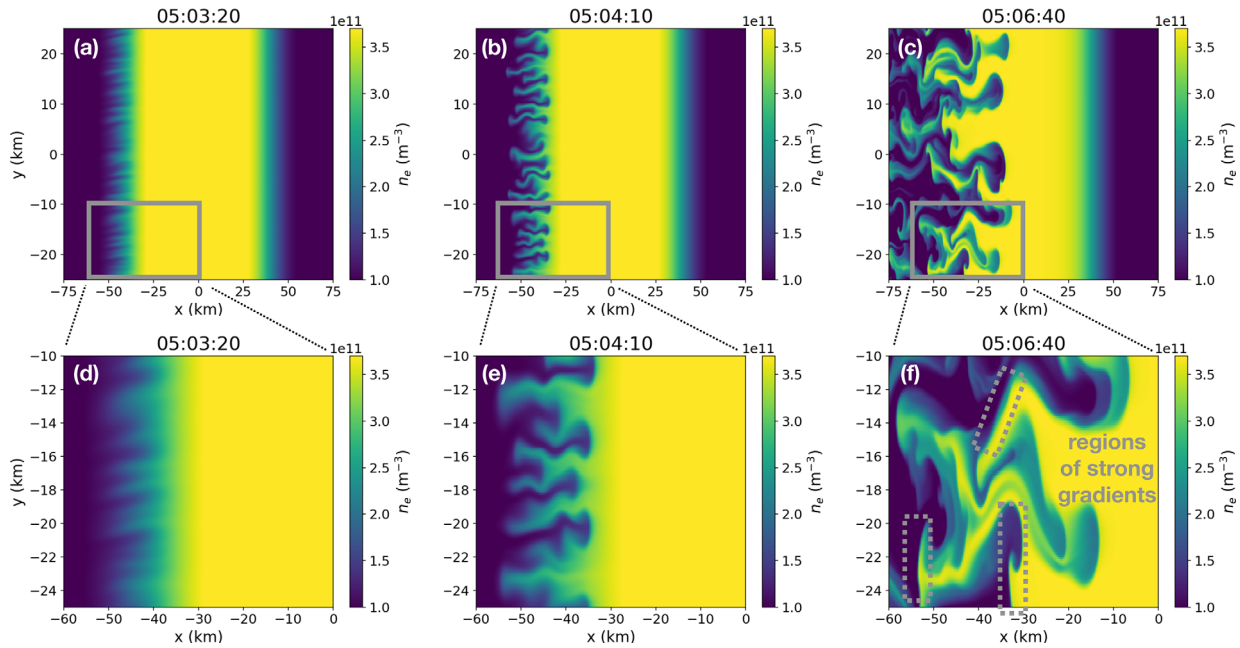
Fig. 3. Output from GEMINI simulation an altitude slice around 300 km at several times as the instability progresses. Panels a, b, and c show the full simulation area, while panels d, e, and f are zoomed-in views to highlight small-scale structuring and sharp gradients.

with 1% of the amplitude of the local background density (n_{e0}). The simulation is run for a total of 480 s from this initial condition, with output density data being generated every 0.5 s to input to SIGMA.

Figure 3 shows snapshots of the plasma density in the x–y plane at about 300 km altitude. Structures are visibly present at around 200 s into the simulation (Figs. 3a and 3d), and fully developed finger-like structures form by 240 s (Figs. 3b and 3e). These develop into structures with very sharp gradients as the instability progresses to times where we evaluate the scintillation (>300 s, Figs. 3c and 3f). By the final stage of the simulation, depicted partly in Figure 3f, there are very clear and large (i.e., >100%) variations in plasma density over distances of ≤1 km – commensurate with Fresnel scales of interest for our data. An animation of the GEMINI density output from the entire simulation is available in the Supplemental Material (S2). Such structures are a natural part of the nonlinear variation of GDI, where structures tend to steepen on their trailing edge leading to, effectively, the formation of contact discontinuities in density (Deshpande et al., 2021).

It is noted here that our models are not yet able, given current software and computational capabilities, to resolve diffusive scales (~decameter) that likely stabilize GDI (Lamarche et al., 2020), so part of the irregularity spectrum will necessarily be unresolved, which will affect modeled scintillation to an extent. However, we are still able to resolve Fresnel scales for VHF and UHF signals from the CERTO beacons and (to a somewhat lesser extent) for an L1 signal from CHAIN. Thus these simulations still provide useful insight into the initiation and growth of plasma instability and its connection to observed scintillation signals in our data.

The 3D electron density generated by GEMINI is fed into SIGMA to predict the power and phase of the scintillation signal on the ground (Deshpande et al., 2014; Deshpande & Zettergren, 2019). In order to obtain theoretical context for

the multi-frequency, multi-scale observational study presented in this paper, we performed SIGMA simulations at L1, UHF, and VHF to match the three observational signals observed at Resolute Bay. For simplicity, we only show one representative L1 SIGMA run with an IPP passing through most parts of the patch. This will be compared with the three observed CHAIN L1 signals, which pass through the interior, exterior, and trailing edge of the patch. In order to avoid memory issues on a standard high-performance computer cluster, we simulate 60 s long time series with a 10 Hz sampling frequency. SIGMA takes in GEMINI density patterns at 05:05:50, which is late in the run when small-scale structuring has developed and permeated the patch (a minute before the instance shown in Fig. 3c). This stage was chosen because, at the measured plasma drift velocity, it would have taken on the order of 10s minutes for the patch to travel from the cusp (where it was assumed to be created) to RBO. We confirmed this choice by performing propagation simulations at earlier times as well as later times in the simulations (not shown in this paper), where the strengths of the simulated signal were much lower. We also did a study with a lower resolution (~200 m) of GEMINI runs and found that SIGMA simulated results were not sufficiently capturing the scintillation, thus we generated the highest resolution GEMINI run presented in this paper. For UHF and VHF SIGMA simulations, we apply spherical wave propagation correction because waves transmitted from a low-Earth orbit no longer satisfy the plane wave assumption at ionospheric altitudes that otherwise is applicable for GPS transmissions.

5 Data-model comparison

Finally, we qualitatively compare the SIGMA output of predicted fluctuations with the actual signal fluctuations measured by ground receivers in the vicinity of Resolute Bay.
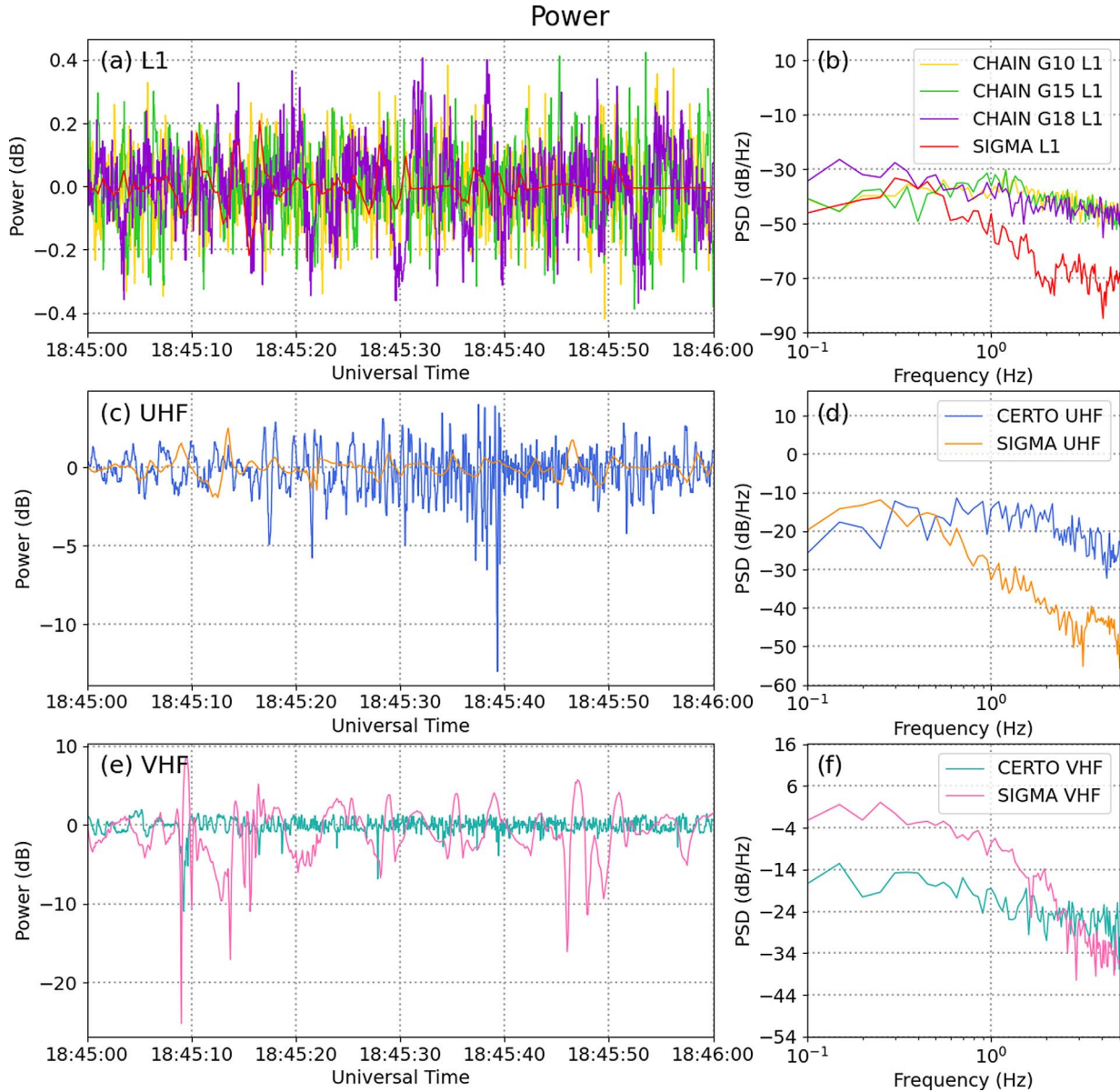
Power

Fig. 4. Signal power time series and PSDs of both observed and simulated dates for L1 (panels a and b), UHF (panels c and d), and VHF (panels e and f).

Figures 4 and 5 show the detrended signal perturbations as measured by the CHAIN and CERTO receivers and the predicted perturbations from GEMINI-SIGMA simulations. We apply a 5-point median filter to the 50 Hz observed CHAIN and CERTO data to ease comparison with the 10 Hz simulated data. Although 10 Hz is not sufficient to capture all the dynamics related to scintillation, previous studies have indicated that a 10 Hz sampling rate is enough to capture most of the signal fluctuations (Deshpande & Zettergren, 2019). Figure 4 shows the detrended power of the L1, UHF, and VHF signals (Figs. 4a, 4c, and 4e, respectively). Figures 4b, 4d, and 4f show the power spectral densities (PSD) of the L1, UHF, and VHF signals, respectively. Figure 5 shows the detrended absolute L1 phase (Fig. 5a) and relative VHF phase (Fig. 5c), as well as the corresponding L1 (Fig. 5b) and VHF (Fig. 5d) PSDs.

SIGMA returns the absolute phase for all frequencies, but to ease comparison with the relative phase measured by the CERTO receiver, the VHF phase relative to the UHF phase is calculated based on Bernhardt and Siefring (2006, Eq. (2)).

Note that due to the stochastic nature of irregularity development and scintillation, we do not expect the SIGMA results to match the observed CHAIN or CERTO time series. Rather, we look for similarities in the peak-to-peak amplitude of the signals as well as the PSD. SIGMA L1 power (Fig. 4a) has distinctly smaller perturbations than any of the three CHAIN time series, however even the measured perturbations are extremely low-amplitude and likely do not indicate significant plasma irregularities. Both the time series (Fig. 4a) and the PSDs (Fig. 4b) of all three CHAIN signals are extremely similar, indicating that for this event, there is minimal plasma structuring at
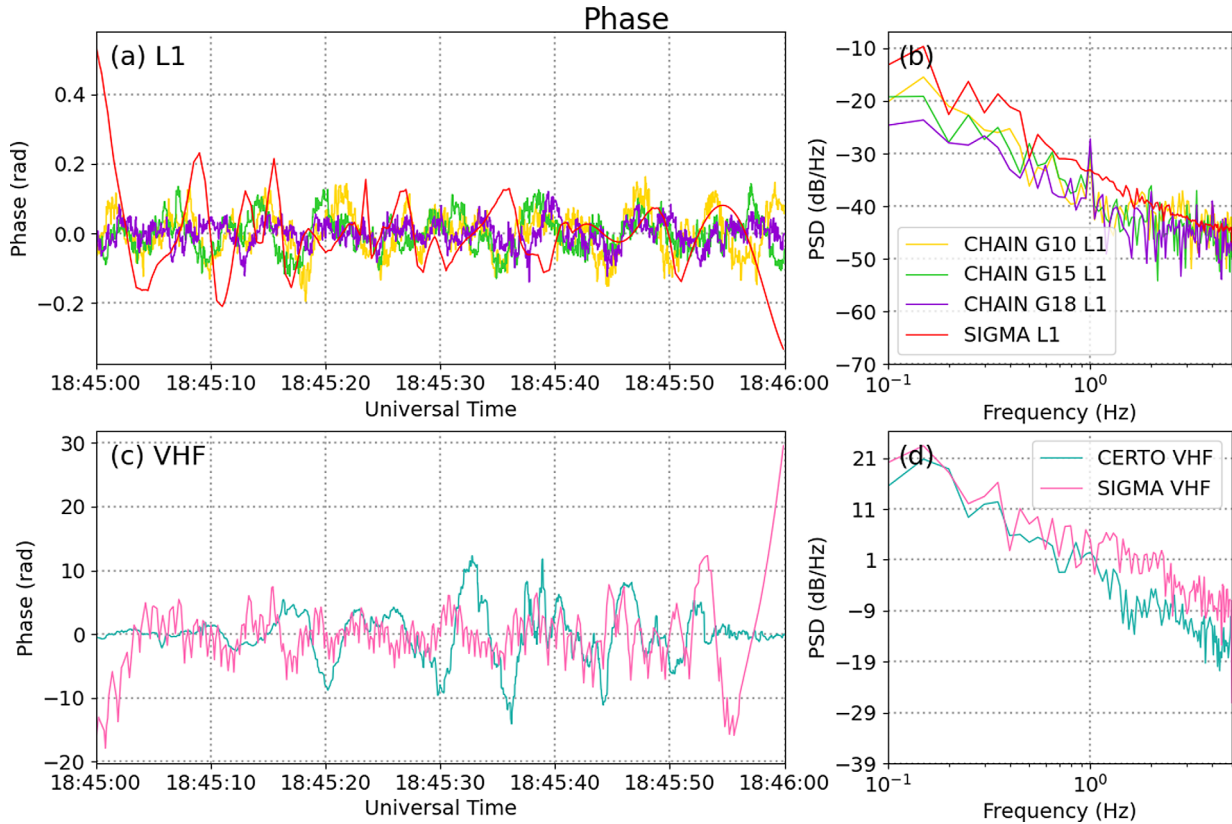
Fig. 5. Signal phase time series and PSDs of both observed and simulated date for L1 (panels a and b) and VHF (panels c and d). Note that the L1 signal is absolute phase while the VHF signal is relative phase.

the L1 Fresnel scale in and around the patch. The SIGMA results for UHF power (Fig. 4c) approximately match the amplitude of the CERTO perturbations for some parts, but not all, of the time series. However, the SIGMA fluctuations in VHF power (Fig. 4e) generally overestimate the CERTO fluctuations and have a longer period, leading to as steeper PSD (Fig. 4f). This is thought to be due in part to GEMINI under resolving the smallest scale features, which systematically reduces the power in the high-frequency end of the PSD. Both the L1 and VHF phase time series (Figs. 5a and 5c) have some regions where the peak-to-peak SIGMA amplitude is similar to the observed scintillation.

The PSD spectra from both the SIGMA simulations and the CHAIN/CERTO observations appear similar in most cases, but they can be challenging to compare directly. We want to reiterate that this is a qualitative comparison. The simulated and observed PSDs of phase (Fig. 5) match better compared to those of power (Fig. 4). The VHF phase PSDs show particularly good agreement at lower frequencies (Fig. 5d). Observed power PSDs appear much flatter, possibly due to the presence of a high-frequency noise-like signal. At L1 frequencies, both phase and power time series show minimal fluctuations (note the small y-axis ranges). The noise floors for observed L1 power and phase start between 1 and 2 Hz (Figs. 4b and 5b), which could result from a combination of high velocities and lack of close-to-Fresnel scale size structures. Although power drops for simulated time series go up in strength with lower frequencies as expected, SIGMA simulations may need scrutiny to determine

if propagation at lower frequencies is creating any artifacts in power.

6 Discussion

Although we have based our GEMINI simulation on RISR measurements, several parameters were effectively unconstrained and had to be specified in an *ad hoc* fashion. Moreover, it is relatively straightforward to argue that these specifications/ assumptions impact the development of plasma irregularities and motivate future experiments studying irregularity formation and its effects on radio propagation.

The most significant assumption made in our modeling is likely the initial gradient scale length, $\ell = n/|\nabla n| = 10$ km, along the edge of the polar patch. In an ideal geometry (local, planar), the linear growth rate for GDI is $\gamma = v_0/\ell$, and the gradient scale length strongly impacts the rate of irregularity development into a nonlinear regime (Keskinen & Ossakow, 1981; Gondarenko & Guzdar, 2006a). If a gradient scale of 100 km (rather than 10 km) is assumed, irregularity development will be approximately 10 times slower. To visualize this, compare the GEMINI output (from Supplemental Material (S2)) at 05:05:50 (350 s into the simulation), which is the late stage that was fed into SIGMA, and at 05:00:35 (35 s into the simulation), which is the expected state of development at the end of the simulation if it had been started with $\ell = 100$ km. At this stage, GEMINI has yet to develop any visible perturbations that could generate

scintillation. To develop scintillation-scale structures on a reasonable time scale, a larger growth rate (and sharper initial gradient) is needed. Unfortunately, RISR's ~58 km-beam separations at F-region altitudes cannot directly resolve the sharp edge gradients expected to drive GDI. The choice of $\ell = 10$ km in this study is both consistent with the growth time scales we expect for this event and comparable to the gradient scale lengths assumed in other modeling studies (Guzdar et al., 1998; Gondarenko & Guzdar, 1999, 2004a, 2004b, 2006a). However, a major need for future studies is to find better observational constraints for the scale length ℓ.

We also do not know what type of additional internal or edge structuring the patch possessed when its formation in the cusp. Resolute Bay is well within the polar cap, so we have no direct cusp observations for this event. We have assumed that the dayside plasma is relatively smooth with small, noise-like broadband perturbations in our models. One can easily imagine a very different situation where a pre-existing large-scale structure within the patch and/or uneven gradients affect growth. There have been some direct observations of patch formation with cusp incoherent scatter radars (Oksavik et al., 2006; Ren et al., 2020; Nishimura et al., 2021), as well as in situ sounding rocket measurements that demonstrate sub-kilometer initial structuring on polar cap patches (Lorentzen et al., 2010; Moen et al., 2012; Oksavik et al., 2012). These studies support our initial assumed 10 km gradient scale length, but it is still challenging to determine appropriate seed structuring.

Ultimately, the initial gradient scale length and noise-like seeding choices are poorly constrained by the currently available data and difficult to fully justify, and we know that these are significant factors controlling the formation of irregularities and scintillation. By nature, small variations in linear growth conditions can lead to very different system behavior, and this fact is borne out in our simulations. Future work will explore the use of new observational techniques to establish a better range of values for these parameters – effectively constraining parameter spaces to guide further simulation and theoretical work.

Due to the lack of direct cusp measurements, we can only estimate the patch's path across the polar cap and approximate the time between patch formation and its appearance over RBO. We assume this is a classic cold-plasma patch formed from dayside photoionized plasma being pulled into the cusp by the polar convection pattern (Cowley et al., 1991; Lockwood & Carlson, 1992; Zhang et al., 2017). It is (very roughly) estimated that the patch is about 10 min old when it is directly over RISR based on the local convection pattern and distance between RBO and the cusp, however, the GEMINI simulation only runs for 8 min due to computation constraints and exhibits robust turbulence for a substantial part of that runtime. When running SIGMA, we use the last 2.5 min of the GEMINI run to characterize the irregularity region, so we are as close as possible to the actual state of the patch, but this does introduce some additional uncertainty in the expected state of internal structuring in the patch during the observation period. Because both the patch age and initial structuring (discussed above) are effectively unconstrained by data, one could come up with a number of gradient and time parameters where the model would show robust irregularities and scintillation.

The GEMINI simulation in this study was initialized with an ideal "tubular" patch (i.e., elongated in the y-direction in our simulation) this approximation allows boundary conditions in the y-direction of the simulation to be cyclic, which avoids edge artifacts. However, the fact that RISR can image the actual morphology of the patch in 3D shows us that there is a potentially substantial structure in the patch-tangent direction that the modeling has not captured. Future work will attempt to address this issue and model a realistically-shaped polar cap patch, but this will require larger simulation domains, such that edge effects do not affect the instability development or novel treatments of boundary conditions to alleviate related artifacts. This issue and the fact that we are not resolving diffusive scales, in particular, demonstrates the technical challenges faced by studies that attempt to model scintillation directly as we do.

Finally, we return briefly to the issue of the role that model resolution plays in features of simulated irregularities. Recent studies have shown that interchange instabilities like GDI can be quite sensitive to model resolution – e.g., it is intuitively clear that this is the case if a model does not resolve dissipative processes, either through lack of resolution or physics, like cross-field diffusion that halts cascade to ever-smaller scales (Deshpande et al., 2021). Simulation of the saturated/turbulent state of the instability, wherein diffusive scales need to be resolved, incurs a high computational cost and is left to a future study focused on the modeling and theoretical aspects of the irregularities.

Although there are many challenges with accurately initializing GEMINI based on direct observations, our modeling shows that plasma turbulence is plausibly present during this event and that it can explain, to a degree, the frequency-dependent radio scintillation that is observed. We can specify the patch interior and exterior densities based on RISR observations and the approximate patch drift velocity (e.g., averaged over the RISR field-of-view). As such, we feel that our modeling is an important step forward from foundation studies like Gondarenko & Guzdar (2006a) and Deshpande & Zettergren (2019), which focused on the basic physics of the instabilities but unconstrained by direct F-region patch measurements afforded by RISR.

The proper treatment of scintillation data at high latitudes is an open question. The main goal of filtering scintillation data is to remove large-scale variations that include satellite motion and low-frequency tropospheric effects. This is typically done by applying a high-pass filter with the Fresnel frequency as the cutoff, however, 0.1 Hz (the traditional cutoff frequency) is only a reasonable value if the plasma is approximately stationary relative to the IPP velocity (Beach, 2006; Jayachandran et al., 2017; Wang et al., 2018). This generally removes refractive effects from large-scale structures while leaving diffractive and refractive effects from structures close to the Fresnel scale. At high latitudes, plasma velocities on the order of 1 km/s are routinely observed, so "stationary plasma" is not a safe assumption (Spogli et al., 2022). Amplitude fluctuations diminish rapidly at scales larger than the Fresnel scale, while phase fluctuations are still apparent. The phase fluctuations can either be due to refractive bending effects in the regions of large spatial gradients or rapid changes in phase advance as the signal LoS moves through the plasma. These resulting phase fluctuations are considered to be equivalent to variations in the LoS total electron content (TEC) (Kintner et al., 2007), but it is challenging to differentiate these from diffractive perturbations in the signal. This results in the filtered phase containing both diffractive and refractive components, which can lead to phenomena

such as the so-called "phase without amplitude scintillation" (Forte & Radicella, 2002; Spogli et al., 2009; Prikryl et al., 2013; Jin et al., 2015; McCaffrey & Jayachandran, 2019). This is not a straightforward effect to correct for, and a variety of approaches have been proposed, but there is presently no generally accepted solution (Forte, 2005; Mushini et al., 2012; Tinin, 2015; Ghobadi et al., 2020; Spogli et al., 2022). Since we are interested in seeing fluctuations in phase and amplitude irrespective of the effect (diffractive vs. refractive), we are not applying any advanced filtering criteria to our analysis.

One of the most interesting results from this study is the clear UHF and VHF signal perturbations observed in the vicinity of the patch despite no significant L1 perturbations from any of the three CHAIN satellites (Figs. 4 and 5). This indicates that there are likely plasma structures at the VHF and UHF Fresnel scales, particularly within and on the trailing edge of the polar cap patch; however, there is no evidence of similar structures at the L1 Fresnel scale anywhere in or around the patch, suggesting that the spectrum of plasma irregularities does not continue all the way down to L1 Fresnel scales. The patch may not be fully structured by the time it was observed over RBO, and structuring at the L1 Fresnel scale will develop as the patch continues to propagate. It is challenging to determine the exact state of patch development from the available observations, however, SIGMA also did not predict significant L1 scintillation even using the late-stage GEMINI output. Alternatively, there could be some other processes or mechanisms responsible for structuring this patch beyond GDI. There is no indication of strong local shears in the RISR velocity data, and the statistical convection patterns for the conditions of this event indicate the patch should continue to move across the polar cap in uniformly-flowing plasma. The available data cannot completely rule out auroral arcs or a sporadic-E layer, but the patch is a "classic" or "cold" patch (interior electron temperature less than the background electron temperature, Table 1), suggesting that F-region particle precipitation is not a large factor (Zhang et al., 2017). Some variety of turbulent or multi-stage mechanisms could still be active (Kelley & Kintner, 1978; Carlson et al., 2007; Burston et al., 2010). Finally, it is possible that there is some aspect of the nonlinear instability development that causes the turbulent cascade to "cutoff" or stabilize at a particular scale under certain conditions. All of these options should be investigated in detail in future work, but we would like to emphasize that the results of this case study show one example of how plasma density structures develop around a polar cap patch but should not be interpreted as a general trend for all patches.

7 Conclusion

This study models the plasma irregularity development and scintillation around an observed polar cap patch and qualitatively compares simulation output with direct measurements of multi-frequency scintillation in the region. We find perturbations in the observed UHF and VHF signals, indicative of plasma structuring at the UHF and VHF Fresnel scales, but no comparable fluctuations in the L1 signal. This suggests that L1 Fresnel scale plasma structures are not present in or around this patch despite the fact that larger structures are, indicating the GDI nonlinear turbulent cascade has not fully developed

to the smallest scales in this patch's lifetime (~10 min), or there are stabilization factors that prevent the cascade from developing below a minimum "cutoff" scale. Further work is required to conclusively determine what physical processes might contribute to these modifications to the turbulent cascade. The simulated and observed scintillation time series often have comparable peak-to-peak amplitudes, but there can be significant differences in the PSDs. This, along with open questions regarding the spectrum of irregularities produced by plasma instability mechanism and small-scale physics, highlights the need for more detailed modeling work in the future. Despite this, this study represents an important step in grounding physics-based simulations with direct measurements of local plasma parameters and interpreting the output in relation to local observations.

Supplementary material

Supplementary material is available at https://www.swsc-journal.org/10.1051/swsc/2022023/olm.

Supplementary Material (S1): Animation of RISR observations of the polar cap patch used in this case study. Format matches Figure 1.

Supplementary Material (S2): Animation of GEMINI simulation output at an altitude slice around 300 km. Format similar to top row of Figure 3.

References

Bahcivan H, Tsunoda R, Nicolls M, Heinselman C. 2010. Initial ionospheric observations made by the new Resolute incoherent scatter radar and comparison to solar wind IMF. *Geophys Res Lett* **37**: L15103. https://doi.org/10.1029/2010GL043632.

Beach TL. 2006. Perils of the GPS phase scintillation index (σ_ϕ). *Radio Sci* **41**(5): RS5S31. https://doi.org/10.1029/2005RS003356.

Bernhardt PA, Siefring CL. 2006. New satellite-based systems for ionospheric tomography and scintillation region imaging. *Radio Sci* **41**: RS5S23. https://doi.org/10.1029/2005RS003360.

Burston R, Astin I, Mitchell C, Alfonsi L, Pedersen T, Skone S. 2010. Turbulent times in the northern polar ionosphere? *J Geophys Res* **115**: A04301. https://doi.org/10.1029/2009JA014813.

Burston R, Mitchell C, Astin I. 2016. Polar cap plasma patch primary linear instability growth rates compared. *J Geophys Res Space Phys* **121**: 3439–3451. https://doi.org/10.1002/2015JA021895.

Carlson HC, Pedersen T, Basu S, Keskinen M. 2007. Case for a new process, not mechanism, for cusp irregularitiy production. *J Geophys Res* **112**: A11304. https://doi.org/10.1029/2007JA012384.

Coker C, Bust GS, Doe RA, Gaussiran TL. 2004. High-latitude plasma structure and scintillation. *Radio Sci* **39**: RS1S15. https://doi.org/10.1029/2002RS002833.

Coley WR, Heelis RA. 1998. Structure and occurrence of polar ionization patches. *J Geophys Res* **103(A2)**: 2201–2208. https://doi.org/10.1029/97JA03345.

Costa E, Kelley MC. 1977. Ionospheric scintillation calculations based on in situ irregularity spectra. *Radio Sci* **12**: 797–809. https://doi.org/10.1029/RS012i005p00797.

Cowley SWH, Freeman MP, Lockwood M, Smith M. 1991. The ionospheric signatures of flux transfer events. In: *CLUSTER – dayside polar cusp, vol. ESA SP-330*, ESTEC, Nordvijk, The Netherlands, pp. 105–112.

Crowley G. 1996. Critical review of ionospheric patches and blobs. In: *Review of radio science 1993–1996*, Stone WR (Ed.), Chap. **27**, Oxford Univ. Press, New York, pp. 619–648.

Crowley G, Carlson HC, Basu S, Denig WF, Buchau J, Reinisch BW. 1993. The dynamic ionospheric polar hole. *Radio Sci* **28(3)**: 401–413. https://doi.org/10.1029/92RS02878.

Deshpande K, Zettergren M, Spicher A, Lamarche L, Hirsch M, Redden M. 2021. Modeling high-latitude F-region ionospheric fluid instabilities: Linear and nonlinear evolution and observational signatures. In: *Cross-scale coupling and energy transfer in the magnetosphere-ionosphere-thermosphere system*, Deng Y, Verkhoglyadova O, Zhang S, Nishimura T (Eds.), Chap. **3.2**, Elsevier, Amsterdam, Netherlands, pp. 127–175.

Deshpande KB, Bust GS, Clauer CR, Rino CL, Carrano CS. 2014. Satellite-beacon Ionospheric-scintillation Global Model of the upper Atmosphere (SIGMA) I: High latitude sensitivity study of the model parameters. *J Geophys Res Space Phys* **119**: 4026–4043. https://doi.org/10.1002/2013JA019699.

Deshpande KB, Zettergren MD. 2019. Satellite-Beacon Ionospheric-Scintillation Global Model of the Upper Atmosphere (SIGMA) III: Scintillation simulation using A physics-based plasma model. *Geophys Res Lett* **46(9)**: 4564–4572. https://doi.org/10.1029/2019GL082576.

Forte B. 2005. Optimum detrending of raw GPS data for scintillation measurements at auroral latitudes. *J Atmos Sol-Terr Phys* **67(12)**: 1100–1109. https://doi.org/10.1016/j.jastp.2005.01.011.

Forte B, Radicella SM. 2002. Problems in data treatment for ionospheric scintillation measurments. *Radio Sci* **37**: 1096. https://doi.org/10.1029/2001RS002508.

Ghobadi H, Spogli L, Alfonsi L, Cesaroni C, Cicone A, Linty N, Romano V, Cafaro M. 2020. Disentangling ionospheric refraction and diffraction effects in GNSS raw phase through fast iterative filtering technique. *GPS Solut* **24(85)**. https://doi.org/10.1007/s10291-020-01001-1.

Gillies RG, van Eyken A, Spanswick E, Nicolls M, Kelly J, et al. 2016. First observations from RISR-C incoherent scatter radar. *Radio Sci* **51**: 1645–1659. https://doi.org/10.1002/2016RS006062.

Gondarenko N, Guzdar P. 1999. Gradient drift instability in high latitude plasma patches: Ion inertial effects. *Geophys Res Lett* **26(22)**: 3345–3348. https://doi.org/10.1029/1999GL003647.

Gondarenko N, Guzdar P. 2004a. Density and electric field fluctuations associated with the gradient drift instability in the high-latitude ionosphere. *Geophys Res Lett* **31(11)**. https://doi.org/10.1029/2004GL019703.

Gondarenko N, Guzdar P. 2004b. Plasma patch structuring by the nonlinear evolution of the gradient drift instability in the high-latitude ionosphere. *J Geophys Res Space Phys* **109(A9)**. https://doi.org/10.1029/2004JA010504.

Gondarenko NA, Guzdar PN. 2006a. Nonlinear three-dimentional simulations of mesoscale structuring by multiple drives in high-latitude plasma patches. *J Geophys Res* **111**: A08302. https://doi.org/10.1029/2006JA011701.

Gondarenko NA, Guzdar PN. 2006b. Simulations of the scintillation-producing irregularities in high-latitude plasma patches. *Geophys Res Lett* **33(22)**. https://doi.org/10.1029/2006GL028033.

Guzdar P, Gondarenko N, Chaturvedi P, Basu S. 1998. Three-dimensional nonlinear simulations of the gradient drift instability in the high-latitude ionosphere. *Radio Sci* **33(6)**: 1901–1913. https://doi.org/10.1029/98RS01703.

Heinselman CJ, Nicolls MJ. 2008. A Bayesian approach to electric field and E-region neutral wind estimation with the Poker Flat Advanced Modular Incoherent Scatter Radar. *Radio Sci* **43**: RS5013. https://doi.org/10.1029/2007RS003805.

Hosokawa K, Shiokawa K, Otsuka Y, Ogawa T, St-Maurice J-P, Sofko GJ, Andre DA. 2009. Relationship between polar cap patches and field-aligned irregularities as observed with an all-sky airglow imager at Resolute Bay and the PolarDARN radar at Rankin Inlet. *J Geophys Res* **114**: A03306. https://doi.org/10.1029/2008JA013707.

Hosokawa K, Taguchi S, Ogawa Y. 2016. Edge of polar cap patches. *J Geophys Res Space Phys* **121**: 3410–3420. https://doi.org/10.1002/2015JA021960.

Huba J, Mitchell H, Keskinen M, Fedder J, Satyanarayana P, Zalesak S. 1988. Simulations of plasma structure evolution in the high-latitude ionosphere. *Radio Sci* **23(4)**: 503–512. https://doi.org/10.1029/RS023i004p00503.

Jayachandran PT, Hamza AM, Hosokawa K, Mezaoui H, Shiokawa K. 2017. GPS amplitude and phase scintillation associated with polar cap auroral forms. *J Atmos Sol-Terr Phys* **164**: 185–191. https://doi.org/10.1016/j.jastp.2017.08.030.

Jayachandran PT, Langley RB, MacDougall JW, Mushini SC, Pokhotelov D, et al. 2009. Canadian high arctic ionospheric network (CHAIN). *Radio Sci* **44**: RS0A03. https://doi.org/10.1029/2008RS004046.

Jin Y, Moen JI, Miloch WJ. 2014. GPS scintillaiton effects associated with polar cap patches and substorm auroral activity: direct comparison. *J Space Weather Space Clim* **4**: A23. https://doi.org/10.1051/swsc/2014019.

Jin Y, Moen JI, Miloch WJ. 2015. On the collocation of the cusp aurora and the GPS phase scintillation: A statistical study. *J Geophys Res Space Phys* **120(10)**: 9176–9191. https://doi.org/10.1002/2015JA021449.

Jin Y, Moen JI, Oksavik K, Spicher A, Clausen LBN, Miloch WJ. 2017. GPS scintillations associated with cusp dynamics and polar cap patches. *J Space Weather Space Clim* **7**: A23. https://doi.org/10.1051/swsc/2017022.

Kelley MC, Kintner PM. 1978. Evidence for two-dimensional inertial turbulence in a cosmic-scale low-β plasma. *Astrophys J* **220**: 339–345. https://doi.org/10.1086/155911.

Kelly J, Heinselman CJ. 2009. Initial results for Poker Flat Incoherent Scatter Radar (PFISR). *J Atmos Sol-Terr Phys* **71**: 635. https://doi.org/10.1016/j.jastp.2009.01.009.

Keskinen MJ, Ossakow SL. 1981. On the spatial power spectrum of the $E \times B$ gradient drift instability in ionospheric plasma clouds. *J Geophys Res* **86**: 6947–6950. https://doi.org/10.1029/JA086iA08p06947.

Kintner PM, Ledvina BM, de Paula ER. 2007. GPS and ionospheric scintillations. *Space Weather* **5**: S09003. https://doi.org/10.1029/2006SW000260.

Kivanç O, Heelis RA. 1997. Structure in ionospheric number density and velocity associated with polar cap ionization patches. *J Geophys Res* **102(A1)**: 307–318. https://doi.org/10.1029/96JA03141.

Knepp DL. 1983. Multiple phase-screen calculation of the temporal behavior of stochastic waves. *Proc IEEE* **71**: 722–737. https://doi.org/10.1109/PROC.1983.12660.

Lamarche LJ, Varney RH, Siefring CL. 2020. Analysis of plasma irregularities on a range of scintillation-scales using the resolute bay incoherent scatter radars. *J Geophys Res Space Phys* **125(3)**. https://doi.org/10.1029/2019JA027112.

Linson LM, Workman JB. 1970. Formation of striation in iono-spheric plasma clouds. *J Geophys Res* **75(16)**: 3211–3219. https://doi.org/10.1029/JA075i016p03211.

Lockwood M, Carlson HC. 1992. Production of polar cap electron density patches by transient magnetopause reconnection. *Geophys Res Lett* **19(17)**: 1731–1734. https://doi.org/10.1029/92GL01993.

Lorentzen DA, Moen J, Oksavik K, Sigernes F, Saito Y, Johnsen MG. 2010. In situ measurement of a newly created polar cap patch. *J Geophys Res Space Phys* **115(A12)**.

Makarevich RA. 2014. Symmetry considerations in the two-fluid theory of the gradient-drift instability in the lower ionosphere. *J Geophys Res Space Phys* **119**: 7902–7913. https://doi.org/10.1002/2014JA020292.

McCaffrey AM, Jayachandran PT. 2019. Determination of the refractive contribution to GPS phase "scintillation". *J Geophys Res Space Phys* **124**. https://doi.org/10.1029/2018JA025759.

Milan SE, Lester M, Yeoman TK. 2002. HF radar polar patch formation revisited: Summer and winter variations in dayside plasma structuring. *Ann Geophys* **20**: 487–499. https://doi.org/10.5194/angeo-20-487-2002.

Mitchell H Jr, Fedder J, Keskinen M, Zalesak S. 1985. A simulation of high latitude F-layer instabilities in the presence of magneto-sphere-ionosphere coupling. *Geophys Res Lett* **12(5)**: 283–286. https://doi.org/10.1029/GL012i005p00283.

Moen J, Oksavik K, Abe T, Lester M, Saito Y, Bekkeng TA, Jacobsen KS. 2012. First in situ measurements of HF radar echoing targets. *Geophys Res Lett* **39**: L07104. https://doi.org/10.1029/2012GL051407.

Mushini SC, Jayachandran PT, Langley RB, MacDougall JW, Pokhotelov D. 2012. Improved amplitude- and phase-scintillation indices derived from wavelet detrended high-latitude GPS data. *GPS Solut* **16**: 363–373. https://doi.org/10.1007/s10291-011-0238-4.

Nishimura Y, Sadler FB, Varney RH, Gilles R, Zhang SR, Coster AJ, Nishitani N, Otto A. 2021. Cusp dynamics and polar cap patch formation associated with a small IMF southward turning. *J Geophys Res Space Phys* **126**: e2020JA029090. https://doi.org/10.1029/2020JA029090.

Oksavik K, Moen J, Bekkeng TA, Bekkeng JK. 2012. In situ measurements of plasma irregularity growth in the cusp ionosphere. *J Geophys Res* **117**: A11301. https://doi.org/10.1029/2012JA017835.

Oksavik K, Ruohoniemi JM, Greenwald RA, Baker JBH, Moen J, Carlson HC, Yeoman TK, Lester M. 2006. Observations of isolated polar cap patches by the European Incoherent Scatter (EISCAT) Svalbard and Super Dual Auroral Radar Network (SuperDARN) Finland radars. *J Geophys Res* **111**: A05310. https://doi.org/10.1029/2005JA011400.

Perry GW, St.-Maurice J-P. 2018. A polar-cap patch detection algorithm for the Advanced Modular Incoherent Scatter Radar System. *Radio Sci* **53**: 1225–1244. https://doi.org/10.1029/2018RS006600.

Prikryl P, Ghoddousi-Fard R, Kunduri BSR, Thomas EG, Coster AJ, Jayachandran PT, Spanswick E, Danskin DW. 2013. GPS phase scintillation and proxy index at high latitudes during a moderate geomagnetic storm. *Ann Geophys* **31(5)**: 805–816.

Ren J, Zou S, Gillies RG, Donovan E, Varney RH. 2018. Statistical characteristics of polar cap patches observed by RISR-C. *J Geophys Res Space Phys* **123**: 6981–6995. https://doi.org/10.1029/2018JA025621.

Ren J, Zou S, Kendall E, Coster A, Sterne K, Ruohoniemi M. 2020. Direct observations of a polar cap patch formation associated with dayside reconnection driven fast flow. *J Geophys Res Space Phys* **124**: e2019JA027745. https://doi.org/10.1029/2019JA027745.

Rino CL. 2010. *The theory of scintillation with applications in remote sensing*, John Wiley & Sons, Hoboken, NJ. ISBN 9780470644775. https://doi.org/10.1002/9781118010211, URL http://books.google.com/books?id=TXNZxBfLBrUC.

Shkarofsky IP. 1968. Generalized turbulence space-correlation and wave-number spectrum-function pairs. *Can J Phys* **46**: 2133. https://doi.org/10.1139/p68-562.

Siefring CL, Bernhardt PA, James HG, Parris RT. 2015. The CERTO beacon on CASSIOPE/e-POP and experiments using high-power HF ionospheric heaters. *Space Sci Rev* **189**: 107–122. https://doi.org/10.1007/s11214-014-0110-2.

Sojka JJ. 2013. Ionosphere induced scintillation: A space weather enigma. *Space Weather* **11**: 134–137. https://doi.org/10.1002/swe.20041.

Spicher A, Cameron T, Grono EM, Yakymenko KN, Buchert SC, Clausen LBN, Knudsen DJ, McWilliams KA, Moen JI. 2015. Observations of polar cap patches and calcualtion of gradient drift instability growth times: A Swarm case study. *Geophys Res Lett* **42**: 201–206. https://doi.org/10.1002/2014GL062590.

Spicher A, Deshpande K, Jin Y, Oksavik K, Zettergren MD, Clausen LBN, Moen JI, Hairston MR, Baddeley L. 2020. On the production of ionospheric irregularities via Kelvin-Helmholtz instability associated with cusp flow channels. *J Geophys Res Space Phys* **125(6)**: e2019JA027734. https://doi.org/10.1029/2019JA027734.

Spogli L, Alfonsi L, De Franceschi G, Romano V, Aquino MHO, Dodson A. 2009. Climatology of GPS ionospheric scintillations over high and mid-latitude European regions. *Ann Geophys* **27**: 3429–3437. https://doi.org/10.5194/angeo-27-3429-2009.

Spogli L, Ghobadi H, Cicone A, Alfonsi L, Cesaroni C, Linty N, Romano V, Cafaro M. 2022. Adaptive phase detrending for GNSS scintillation detection: A Case study over Antarctica. *IEEE Geosci Remote Sens Lett* **19**. https://doi.org/10.1109/LGRS.2021.3067727.

Thayyil JP, McCaffrey AM, Wang Y, Themens DR, Watson C, Reid B, Zhang Q, Xing Z. 2021. Global positioning system (GPS) scintillation associated with a polar cap patch. *Remote Sens* **13(10)**. https://doi.org/10.3390/rs13101915.

Tinin MV. 2015. Eliminating diffraction effects during multi-frequency correction in global navigation satellite systems. *J Geod* **89**: 491–503. https://doi.org/10.1007/s00190-015-0794-4.

Tsunoda RT. 1988. High-latitude F region irregularities: A review and synthesis. *Rev Geophys* **26**: 719–760. https://doi.org/10.1029/RG026i004p00719.

Wang Y, Zhang Q-H, Jayachandran PT, Lockwood M, Zhang S-R, Moen J, Xing Z-Y, Ma Y-Z, Lester M. 2016. A comparison between large-scale irregularities and scintillation in the polar ionosphere. *Geophys Res Lett* **43**: 4790–4798. https://doi.org/10.1002/2016GL069230.

Wang Y, Zhang Q-H, Jayachandran PT, Moen J, Xing Z-Y, Chadwick R, Ma Y-Z, Ruohoniemi JM, Lester M. 2018. Experimental evidence on the dependence of the standard GPS phase scintillation index on the ionospheric plasma drift around noon sector of the polar ionosphere. *J Geophys Res Space Phys* **123**: 2370–2378. https://doi.org/10.1002/2017JA024805.

Weber EJ, Buchau J, Moore JG, Sharber JR, Livingston RC, Winningham JD, Reinisch BW. 1984. F layer ionization patches in the polar cap. *J Geophys Res* **89**(A3): 1683–1694. https://doi.org/10.1029/JA089iA03p01683.

Yeh KC, Liu CH. 1982. Radio wave scintillations in the ionosphere. *IEEE Proc* **70**: 324–360.

Zettergren MD, Semeter JL, Dahlgren H. 2015. Dynamics of density cavities generated by frictional heating: Formation, distortion, and instability. *Geophys Res Lett* **42**(23): 10120–10125. https://doi.org/10.1002/2015GL066806.

Zettergren MD, Snively JB. 2015. Ionospheric response to infra-sonic-acoustic waves generated by natural hazard events. *J Geophys Res Space Phys* **120**(9): 8002–8024. https://doi.org/10.1002/2015JA021116.

Zhang Q-H, Ma Y-Z, Jayachandran PT, Moen J, Lockwood M, et al. 2017. Polar cap hot patches: Enhanced density structures differetn from the classical patches in the ionosphere. *Geophys Res Lett* **44**: 8159–8167. https://doi.org/10.1002/2017GL073439.